Early View publication on
www.wileyonlinelibrary.com
(issue and page numbers not yet assigned;
citable using Digital Object Identifier – **DOI**)

J. Biophotonics 1–16 (2012) / **DOI** 10.1002/jbio.201200039

Journal of
BIOPHOTONICS

REVIEW ARTICLE

Photonic crystal biosensors towards on-chip integration

Daniela Threm[*,**], *Yousef Nazirizadeh*[*,**], *and Martina Gerken*

Institute of Electrical and Information Engineering, Christian-Albrechts-Universität zu Kiel, Kiel, Germany

Received 6 March 2012, revised 24 April 2012, accepted 2 May 2012
Published online 8 June 2012

Key words: biosensor, photonic crystal, on-chip integration

Photonic crystal technology has attracted large interest in the last years. The possibility to generate highly sensitive sensor elements with photonic crystal structures is very promising for medical or environmental applications. The low-cost fabrication on the mass scale is as advantageous as the compactness and reliability of photonic crystal biosensors. The possibility to integrate microfluidic channels together with photonic crystal structures allows for highly compact devices. This article reviews different types of photonic crystal sensors including 1D photonic crystal biosensors, biosensors with photonic crystal slabs, photonic crystal waveguide biosensors and biosensors with photonic crystal microcavities. Their applications in biomolecular and pathogen detection are highlighted. The sensitivities and the detection limits of the different biosensors are compared. The focus is on the possibilities to integrate photonic crystal biosensors on-chip.

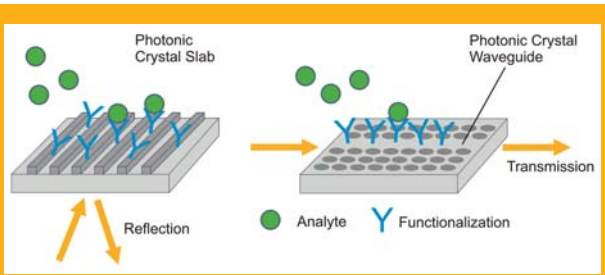

Two different types of optical biosensors with photonic crystal transducers.

1. Introduction

During the past century technical innovations were dominated by the progress in integrated electronics. In this century biotechnology will have a significant value in further improvement of our living standard. Biosensing is one major part of it, which is boosted by new technologies in optics, electronics and material sciences. Biosensors are used in a variety of applications ranging from biomolecular interactions to pathogen detection.

A definition of a biosensor is given by D. Fraser: "A biosensor is an analytical device that incorporates a deliberate and intimate combination of a specific biological element, which creates a recognition event, and a physical element, which transduces the recognition event" [1]. As the specific biological element, nowadays antibodies, aptamers or other molecules are used. These are immobilized on the surface of the physical element, also called the transducer. Here the transducer adopts the functionality of the label and renders the analyte of interest detectable. This is one of the most important properties of biosensors making them faster, simpler and more physiological than their label-based counterparts [2–4].

In an optical detection scheme it has to be considered that the signal strength decreases with decreasing optical path length in the analyte. Therefore, new concepts need to be utilized for signal

* These authors contributed equally to this work.
** Corresponding authors: e-mail: dth@tf.uni-kiel.de, yn@tf.uni-kiel.de, Phone: +00 49 431 8806263, Fax: +00 49 431 8806253

strength optimization in miniaturized optical biosensors. Photonic crystals, which provide local optical modes, are suitable to enhance the light-matter interaction. Photonic crystals were first described by Yablonovitch [5] and John [6] in 1987. They consist of one or more dielectric materials, which are repeated periodically with a period in the range of the photon wavelength. This low-loss periodic dielectric medium can be designed to provide a photonic bandgap. In this optical bandgap light propagation is prohibited for a range of frequencies [7, 8]. On the other hand, photonic crystals also provide optical modes, which localize light inside the structure.

Photonic crystals can be categorized as one-dimensional (1D), two-dimensional (2D) and three-dimensional (3D) photonic crystals depending on the number of directions with a periodic repetition. A 1D photonic crystal consists of a multilayer stack with alternating layers of materials with different dielectric constants [8]. 1D photonic crystals are also known as dielectric mirrors (Bragg mirrors), or as optical filters. A schematic diagram of a 1D photonic crystal biosensor is shown in Figure 1(a). Biosensors based on 1D photonic crystals are reviewed in Section 2.1. All other photonic crystal biosensors developed so far are based on nanostructured slab geometries. Photonic crystal slabs exhibit a periodic structure in one or two directions on the slab surface. In the third direction light is confined by total internal reflection [9]. An example of such a biosensor is shown in Figure 1(b). In Section 2.2 an overview of biosensors using these structures is given. Furthermore, waveguides and cavities may be included in the photonic crystal slab as shown schematically in Figure 1(c) and (d). These structures allow for an enhanced interaction of the light and the analyte. In Section 2.3 and 2.4 the focus is on these structures.

In contrast to other optical methods, which for example measure a layer thickness [10, 11], biosensing with photonic crystals mostly is based on a measurement of a refractive index change due to molecules or pathogens in the vicinity of the photonic crystal. All sensors reviewed in this paper use optical modes partially confined to the photonic crystal, but with an evanescent part extending up to a few hundred nanometers out of the photonic crystal structure. These modes are the origin of resonances or cut-off wavelengths observed in the transmission or reflection spectrum. Refractive index changes in the vicinity of the photonic crystal will influence the mode's effective refractive index. An increase in the effective refractive index results in a red-shift of the resonance or the cut-off wavelength. Therefore, the resonance shift as a function of the bulk refractive index change in the medium surrounding the photonic crystal is suitable as a figure of merit to compare biosensors. The bulk refractive index simulates the presence of biomolecules or pathogens. Furthermore, changing the surrounding refractive index is an experiment, which can be performed reproducibly. However, the detection limit of the biosensor is also a function of the resonance quality factor and system's signal-to-noise ratio. Hence, another figure of merit is the minimal detectable bulk refractive index change. Bulk refractive index measurements do not reflect the real physics in a sensor with a biological recognition element, where depending on the molecule or pathogen of interest, only a few nanometers on the surface are covered. Therefore, the most relevant figure of merit to take into account is the surface mass coverage.

Some decades ago the on-chip integration of electronic devices allowed more powerful and yet more cost-efficient solutions. Today, the on-chip integration of the transducer and biological elements promises the same. Towards on-chip integration it is necessary to assemble fluidic channels in the micrometer range and transducer structures together. Microfluidics is well studied and has the potential to be introduced into many areas of biological analysis [12].

Photonic crystal biosensors offer the potential to be assembled together with microfluidics and are therefore a good platform for on-chip integration [13].

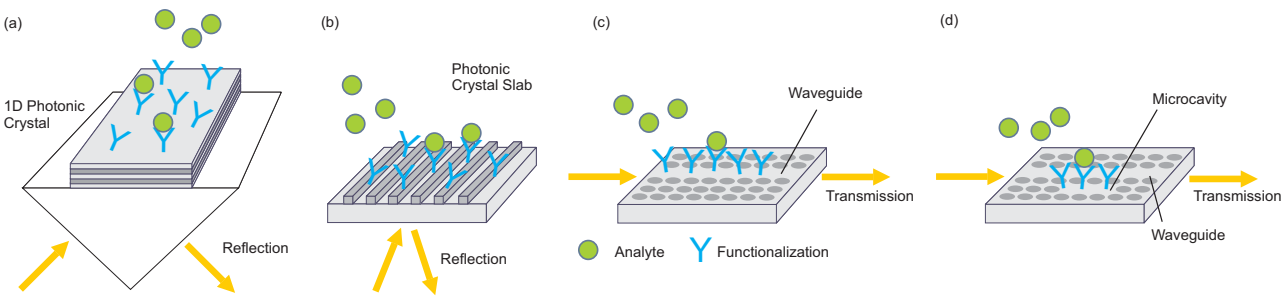

Figure 1 (online color at: www.biophotonics-journal.org) Schematic overview of photonic crystal categories used for biosensors: (**a**) 1D photonic crystals, (**b**) photonic crystal slabs, (**c**) photonic crystal waveguides, and (**d**) photonic crystal microcavities.

This paper is organized as follows: In Section 2 we discuss biomolecular interactions with four different types of photonic crystal biosensors. The discussion of pathogen detection follows in chapter 3. In Section 4 we give examples of different fabrication processes and system demonstrations for on-chip integration. A conclusion is drawn in chapter 5. Biosensors based on photonic crystal fibers are not included in this review.

2. Biomolecular interactions

Label-free detection methods of protein-protein or protein-DNA interactions as well as protein ligand binding are of high interest for diagnostics. Photonic crystal biosensors offer this potential. They are able to detect molecules or pathogen binding with small sample volumes containing low concentrations. In the following sections the four different types of photonic crystal biosensors introduced in Figure 1 and their application possibilities are discussed.

2.1 1D Photonic crystal biosensors

One-dimensional (1D) photonic crystals are thin-film stacks with alternating layers of materials with different dielectric constants (also called Bragg stacks). They provide nonradiative surface waves [14], if excited in the Kretschmann and Otto configuration [15], which is a total internal reflection setup with a prism. These waves exhibit an evanescent part in the direction perpendicular to the surface and are therefore highly sensitive to surface modifications, which is an ideal property for biosensing applications. Villa et al. [16] show the potential of such a configuration as a sensor for thin layers. They demonstrate that a few periods are sufficient for such a sensor.

Konopsky et al. [17] go a step further and employ two surface waves supported by the same 1D photonic crystal for biosensing. The penetration depth of one of the waves is much larger than the other one. The detection of both waves allows the simultaneous tracking of the bulk refractive index and the thickness of an adherent layer. This allows isolating these two parameters and gaining a higher sensitivity for biomolecular detection. The authors also claim that the knowledge about the bulk refractive index can be applied for temperature determination of the analyte. They perform biological binding experiments demonstrating the ability to detect the binding of biotin to a streptavidin monolayer. The minimal detectable quantity amounts to 1.3×10^8 biotin molecules corresponding to 50 fg of analyte on the probed spot of 0.1 mm^2.

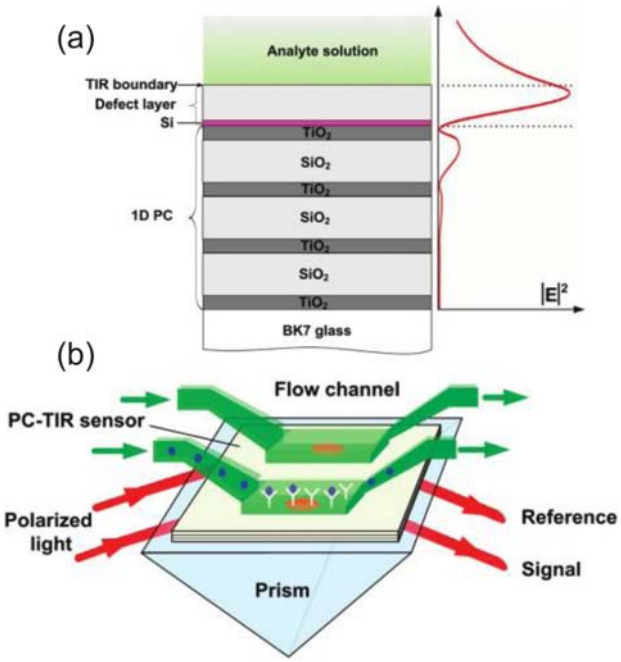

Figure 2 (online color at: www.biophotonics-journal.org) 1D photonic crystal biosensor: On the left side of (**a**) the schematic structure of the 1D photonic crystal is shown. The electric field distribution for light resonant with the structure is shown on the right side. The two dotted lines illustrate the defect layer boundaries. (**b**) Schematic sensor configuration. Two beams of polarized light strike the signal and reference channel. Reprinted with permission from [19]. Copyright 2010, American Chemical Society.

Guo et al. [18, 19] also use 1D photonic crystals, but integrate a defect layer at the top of the thin-film stack. A resonance mode occurs in this defect region, where the field is enhanced as shown in Figure 2(a). This resonance mode exhibits an enhanced electrical field in the vicinity of the surface compared to the surface waves supported by 1D photonic crystals and hence promise higher sensitivities. The authors show the binding of aminopropyl-triethoxysilane (APTES) and glutaraldehyde, which can form thin bilayers to the surface [18]. They estimate a detection limit of 6×10^{-5} nm for molecular layers, which would correspond to 0.06 pg/mm^2 for analyte adsorption. Furthermore, they show the binding of molecules with molecular weights ranging from 244 to 150,000 Da [19]. To obtain a high detection limit, they introduce a reference channel next to the signal channel in the flow cells on top of the 1D photonic crystal (see Figure 2(b)), where two identically polarized beams are used as the excitation source. For bulk solvent refractive index measurements, they obtain a sensitivity of up to 1840 nm/RIU. This is the highest value achieved in any of the photonic crystal sensor types introduced in this review.

2.2 Biosensors with photonic crystal slabs

Photonic crystal slabs are periodically structured high refractive index slabs. These structures provide in-plane guided modes, which cannot couple to the far field. On the other hand, photonic crystal slabs also provide so-called quasi guided modes, which can be scattered out of the slab due to the periodic structure and couple to the far field [20]. Hence, a simple transmission or reflection measurement is sufficient to access these modes, which appear as resonances in the spectrum. These resonances are referred to as guided-mode resonances. The three common types of photonic crystal slabs can be classified as linear, quadratic and triangular photonic crystal slabs [21, 22]. Quadratic and triangular photonic crystal slabs have a periodicity in two directions, while linear photonic crystal slabs show a periodicity in only one spatial direction. Looking at the field profile of guided modes and the quasi guided modes, we observe the field maximum in the high refractive index slab and an evanescent part extending out of the structure. This evanescent part interacts with refractive index changes on the surface, which leads to a shift in the mode's wavelength. When applying the photonic crystal slab as a biosensor, the refractive index change on the surface caused by biomolecule binding events is detected by determining the guided-mode resonance's central wavelength in the reflection or transmission spectrum.

In 2002 Cunningham et al. [23] showed an approach for the detection of molecular interactions. They use the reflection spectrum to determine the guided-mode resonance central wavelength. An LED is used as the light source and the back reflected light is analysed with a spectrometer as shown in Figure 3(a). The binding of molecules on the functionalized surface results in a shift of the resonance wavelength, which is tracked as a function of time and hence delivers a diagram for the molecular interaction. With this setup they demonstrate a detection sensitivity of 0.016 nM/L of streptavidin in PBS corresponding to a 1 ng/ml concentration. As the photonic crystal slab can be fabricated as an extended area, these structures can be applied in a large variety of biological experiments. For instance, Chan et al. [24, 25] show cell cytotoxicity monitoring and Cunningham et al. [26] demonstrated the use of this sensing method for applications in proteomics, where they could demonstrate a mass detection sensitivity of less than 1 pg/mm^2. The possibility to discover inhibitors of protein – DNA interactions is shown in [27]. They demonstrate the large potential of the method: the ability to detect sequence-dependent DNA-binding, sequence-independent DNA-binding and a high-throughput screening. The principle of the protein-DNA binding experiment is shown schematically in Figure 3(b). A streptavidin-coated surface is used to bind biotinylated DNA oligomers. After addition of a blocking agent, a DNA-binding protein is added. This results in a peak wavelength shift in the reflected light.

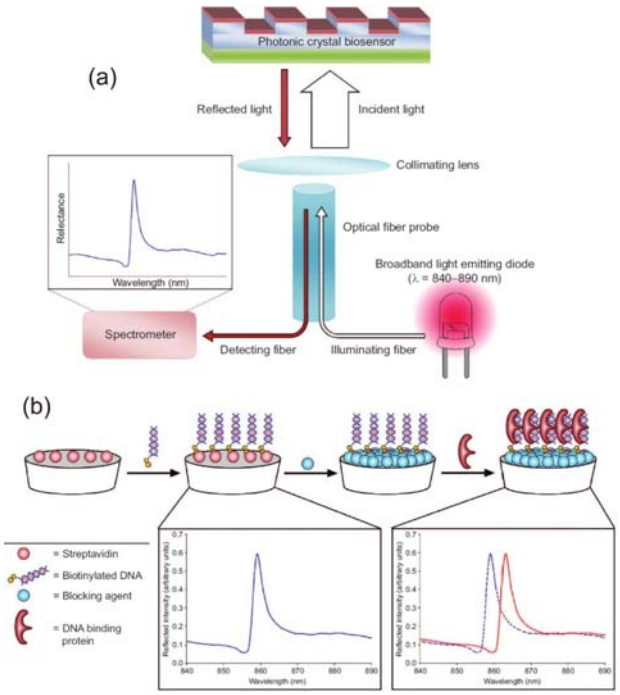

Figure 3 (online color at: www.biophotonics-journal.org) (**a**) Schematic of the working principle of the biosensor. A broadband LED illuminates the photonic crystal slab biosensor from the bottom. The reflected light is transferred to a spectrometer to measure the wavelength shift. (**b**) Schematic diagram of a protein – DNA binding experiment. Photonic crystal biosensors with a streptavidin-coated surface are used to bind biotinylated DNA oligomers. The addition of a DNA-binding protein after a blocking agent is added results in a wavelength shift of a resonance peak in the reflected light. Reprinted with permission from [27]. Copyright 2008, American Chemical Society.

Magnusson et al. [28] utilize the separate consideration of the polarization state. Different resonance peaks appear for incident TE and TM polarization states. Using a polarization filter in the light path, these two modes can be separated and provide an enriched data set, which is useful for increasing the detection accuracy of the given sensor element. As shown in Figure 4 the two polarization states interact differently with the surrounding medium. Thus, a separate reference channel is not necessary to distinguish the variations during data acquisition. Furthermore, El Beheiry et al. [29] suggested that resonances, which extend less to external regions, may be suitable for protein and biomolecule detection (TM resonant mode in Figure 4(a)), as these molecules cover only a few nanometers of the photonic crystal sur-

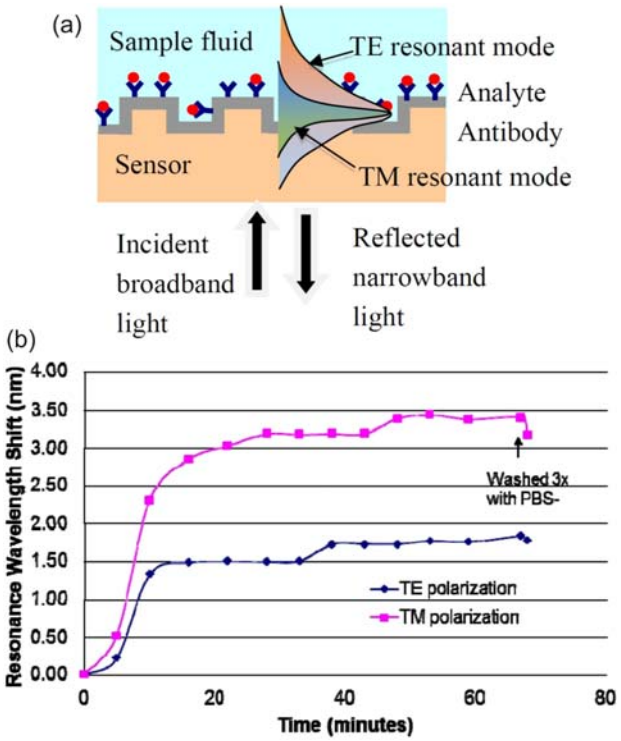

Figure 4 (online color at: www.biophotonics-journal.org) (**a**) Schematic diagram of the two different polarization states incident on the sensor surface. For TE and TM polarization the resonant modes have different mode profiles and occur at different wavelengths. (**b**) Different resonance wavelength shifts for TE and TM polarization as a function of time. The sensor is used to detect the biotin binding (0.5 mg/ml Sulfo-NHS-LC-Biotin) to a silane-coated sensor surface. Reprinted with permission from [28]. Copyright 2011, Multidisciplinary Digital Publishing Institute.

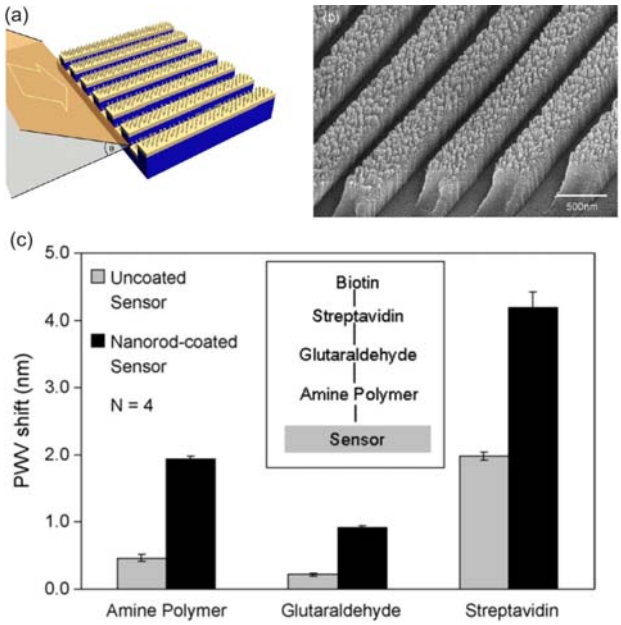

Figure 5 (online color at: www.biophotonics-journal.org) (**a**) Schematic of the set-up of the photonic crystal slab with a nanorod-coated surface and (**b**) SEM image of the surface. (**c**) Enhancement of the peak wavelength shift for nanorod-coated sensors in comparison to uncoated sensors. The shifts are shown for amine polymer, gluteraldehyde and streptavidin. Reprinted from [30], Copyright 2008, with permission from Elsevier.

face. The maximized intersection of the molecule coverage and mode profile will optimize the detection sensitivity. On the other hand, resonances, which extend more to the surrounding medium, are more suitable to detect cells and large analytes (TE resonant mode in Figure 4(a)).

Various approaches to enhance the sensitivity of biosensors with photonic crystal slabs exist. Zhang et al. [30] demonstrate that through the incorporation of a porous TiO_2 film possessing the structure of nanorods into the device, the surface area can be greatly enhanced and a higher functionalization density can be reached. This leads to more biomolecules binding to the surface and results in a higher refractive index change. With this surface modification, they demonstrate an up to $4\times$ sensitivity improvement compared to uncoated sensors (see Figure 5). A similar concept with a different implementation is vertical-sidewall roughness of the photonic crystal slab [31]. Increasing the sensitivity also is shown through the incorporation of low refractive index porous dielectric material into the device structure [32].

Experimental efforts to enhance the sensitivity of photonic crystal slab biosensors are accompanied by theoretical studies. Shi et al. propose to use a photonic crystal slab with spherical voids to capture analytes [33, 34]. They calculate a theoretical sensitivity of 361 nm/RIU.

A higher sensitivity of 510 nm/RIU is obtained experimentally with a free standing photonic crystal slab interacting with small fluid volumes through nano-scale holes in [35]. Ganesh et al. [36] show an improvement of over 4.5 times in the surface-to-bulk-sensitivity ratio through operating at a near-ultraviolet wavelength, as the mode profile is more concentrated on the surface on the photonic crystal slab.

The use of photonic crystal slabs for biosensing requires the tracking of the spectral position of the guided-mode resonance. In the conventional setup this is done using a spectrometer. Here, the limit of detection is a function of wavelength detection accuracy, which can be optimized by a more sophisticated spectrometer and fitting procedures for the resonances. In [37] we propose to use crossed polarization filters in the light path, which cause background

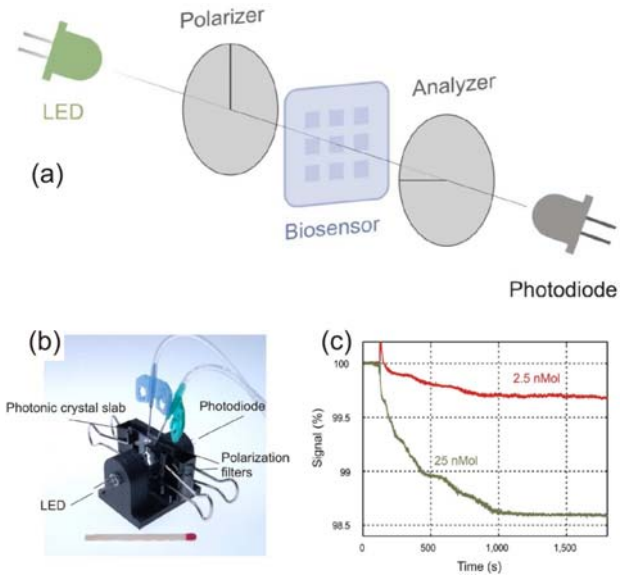

Figure 6 (online color at: www.biophotonics-journal.org) (**a**) Schematic setup of a compact and low-cost biosensing method. An LED and a photodiode are used as the light source and the detector, respectively. The background light, which is not interacting with the photonic crystal surface, is suppressed by the crossed polarization filters. (**b**) Picture of the demonstrator, which is used to perform biomolecule interaction experiments. (**c**) The binding kinetics of streptavidin to biotin is measured with this setup. A 2.5 nMol solution of streptavidin can be detected. Reprinted with permission from [37]. Copyright 2010, Optical Society of America.

suppression and the transmission of only the resonances [38]. Furthermore, the falling edge of the light source (in this case an LED) is matched with the guided-mode resonance wavelength. Hence, any wavelength shift is transferred into an intensity decrease of the resonance, which then can be read out with a standard photodiode. In Figure 6(a) the setup of the experiment is shown. It contains an LED and a photodiode with integrated optics as light source and detector, respectively, and the crossed polarization filters. A demonstrator based on this concept (Figure 6(b)) is able to detect a 2.5 nM streptavidin solution (Figure 6(c)). The limit of detection of this method is defined by the signal-to-noise ratio and the drift of the electronics. The compact and cost-efficient setup makes this method ideal for low-cost applications.

Concluding this section, photonic crystal slabs are advantageous for biosensors as they offer good sensitivities, are able to detect small biomolecule interactions as well as the binding of cells, viruses and bacteria, and are suitable for on-chip integration.

2.3 Photonic crystal waveguide biosensors

A linear waveguide in a photonic crystal (also called photonic crystal waveguide) is formed by introducing a defect line in the lattice structure of a 2D photonic crystal or photonic crystal slab [39, 40] (see Figure 7). This defect line can be created by either removing or changing the size of a single row of holes. A linear waveguide in a photonic crystal slab is especially suitable for biosensing applications. In these structures a given bandwidth of light is guided in the waveguide. This is similar to a conventional core/cladding waveguide structure. Light is confined vertically by total internal reflection of the slab and laterally by the band gap of the 2D photonic crystal structure.

In order to achieve optimal performance, waveguides must satisfy three criteria [39]: First, the waveguide has to support true guided modes, i.e., no leaky modes. Second, in the frequency range of interest the waveguide should be single mode. Third, the guided mode should lie within the bandgap in order to prohibit radiation losses. The third criterion is used in biosensors based on photonic crystal waveguides. The bandgap is strongly influenced by refractive index changes on the surface or at the sidewalls of the holes of the photonic crystal slab. If, for example, the bandgap shifts with increasing refractive index towards longer wavelengths, leaky modes will become guided and the cut-off wavelength of the waveguide is shifted towards longer wavelengths. By

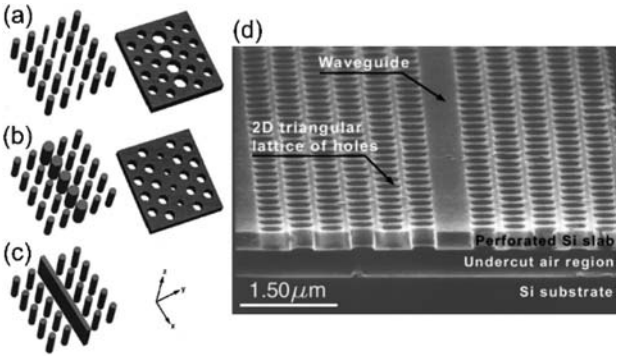

Figure 7 (**a**)–(**c**) Line defects, which generate waveguide modes: (**a**) Reduced-index waveguide created by decreasing or increasing the radius of a line of rods or holes, respectively. (**b**) Increased-index waveguides created by increasing or decreasing the radius of a line of rods or holes, respectively. (**c**) Dielectric-strip waveguide formed by removing a row of rods. Reprinted with permission from [39]. Copyright 2000 by the American Physical Society, http://link.aps.org/. (**d**) SEM image of a waveguide structure in a triangular lattice created by removing a single row of holes. Reprinted with permission from [40]. Copyright 2000, American Institute of Physics.

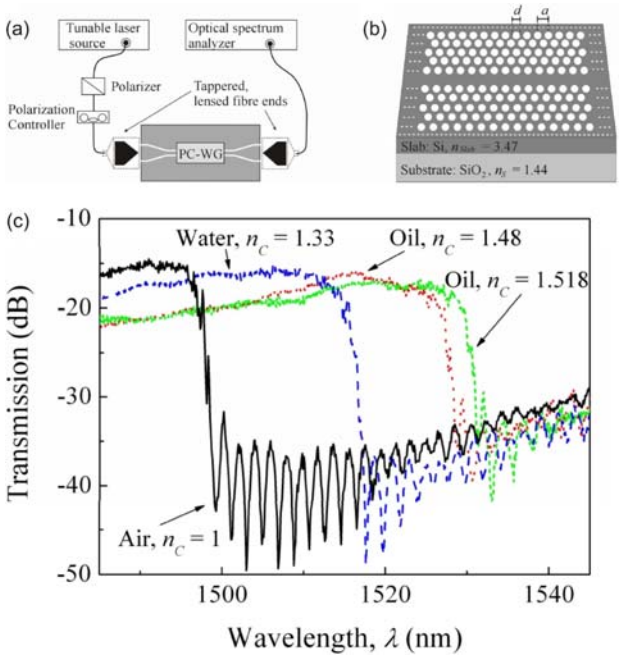

Figure 8 (online color at: www.biophotonics-journal.org) (**a**) Experimental set-up: Tapered, lensed fibers are used to couple light from a laser source into the waveguide on the chip and to the spectrum analyzer. (**b**) Schematic of the photonic crystal waveguide chip. The waveguide is formed by removing one row of holes. (**c**) Transmission spectra measured with the photonic crystal waveguide sensor. Four different media were used: air ($n = 1$), DI-water ($n = 1.33$), and two immersion oils ($n = 1.48$ and $n = 1.518$, respectively). Reprinted with permission from [42]. Copyright 2007, Optical Society of America.

measuring this cut-off wavelength, the refractive index on the surface can be determined, which is changed by binding of molecules.

Beyond that, photonic crystal waveguides have the potential to be applied in an optical circuit, where the light is guided in these waveguides and can be directed to obtain a high degree of integration [40, 41].

Skievesen et al. [42] use a single linear waveguide, which was created by removing a row of holes, and demonstrate refractive index measurements as well as the measurability of protein concentrations. They perform transmission experiments using a tunable laser and an optical spectrum analyser to obtain the cut-off wavelength (Figure 8). With this setup they measure refractive index changes down to $\Delta n = 0.003$. The authors also perform measurements with a bovine serum albumin (BSA) solution with a concentration of 0.15 μM corresponding to 10 μg/ml. They correlate the concentration of the BSA solution with the refractive index of the solution instead of performing biological surface functionalization.

Buswell et al. [43] demonstrate a specific detection of streptavidin to biotin with a photonic crystal waveguide biosensor. The binding of streptavidin to immobilized biotin causes a red-shift of 0.86 nm of the cut-off wavelength for a 2.5 nm streptavidin film. The bulk sensitivity of the shown waveguide biosensor is 88 nm/RIU. To improve the sensitivity the authors investigate a modification in the waveguide sensor. Instead of removing one row of holes, one line of holes is shrunk to a fraction of their original size. A lattice period of $\Lambda = 446$ nm with a hole radius of 0.37Λ for the exterior holes and 0.22Λ for the holes in the waveguide line is used. With this device design the cut-off wavelength is not modified compared to the previous design. Hence, the response is similar except that the modes are shifted to higher frequencies inside the bandgap. However, the advantage of this design is the increased surface area available for sensing in the central high-field region. This modification results in an improvement of the sensitivity up to 120 nm/RIU, which corresponds to an improvement of 40% in comparison to the sensor with a regular waveguide.

Topol'ančik et al. [41] show a multichannel waveguide structure used as a fluid detection scheme. As shown in Figure 9, they use two fluid detection arms having each a row of different shrunk holes, whereas the input waveguide has a row of missing holes as the defect. The bandgap and the waveguide modes are chosen such that only one of the arms transmits light with a particular fluid. Although, they did not show any biosensing applications so far, their sensor potentially can be applied in a biosensor chip, where the presence of a biomolecule can switch between two light paths.

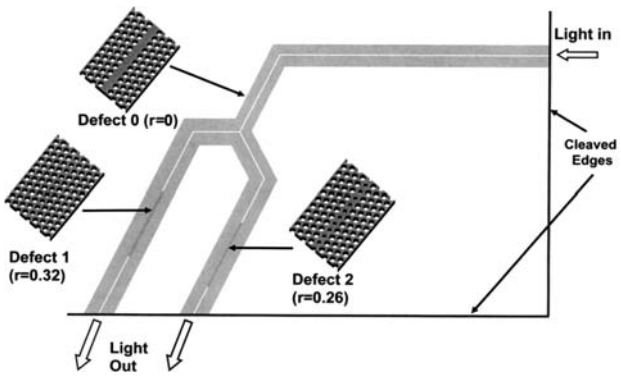

Figure 9 Schematic diagram of a multichannel waveguide structure in a photonic crystal lattice with period Λ. While the input waveguide has a row of missing holes ($r/\Lambda = 0$), the two fluid detection branches have a row of different shrunk holes ($r/\Lambda = 0.32$ and $r/\Lambda = 0.26$, respectively). Reprinted with permission from [41]. Copyright 2003, American Institute of Physics.

2.4 Biosensors with photonic crystal microcavities

Although photonic crystal waveguide biosensors are highly integratable in an optical chip, the readout of the cut-off wavelength tends to be not precise enough for sensitive detection. A photonic crystal microcavity, however, provides resonances with a high quality factor, which are more suitable for sensing applications. By introducing a point defect into the periodic lattice of a photonic crystal structure, a two-dimensional photonic crystal microcavity is formed. This defect can be created either by removing one or more holes or/and by changing the radius of one or more holes. Exemplary, Figure 10(a) shows a microcavity formed by increasing the central hole diameter and removing holes around it. The light can propagate in the photonic crystal, if it is resonant with the defect mode. Hence, the defect mode appears as a high quality resonance within the bandgap on the transmission or reflection spectrum. A common method to measure these resonances is shown in Figure 10(b). The transmission spectrum is obtained using a tunable laser source, which is coupled into a waveguide connected to the microcavity and a detector. The spectral position of the defect mode is highly sensitive to local refractive index changes in its environment, which can be used for biosensors. The higher the refractive index change, the larger the resonance shift towards longer wavelengths.

In biosensing the detection limit of an analyte concentration is one of the most important parameters. For very low concentrations the functionalized sensing area is preferred to be small. Photonic crystal microcavities can be designed to have an effective diameter of only a few microns, which is interacting with the analyte.

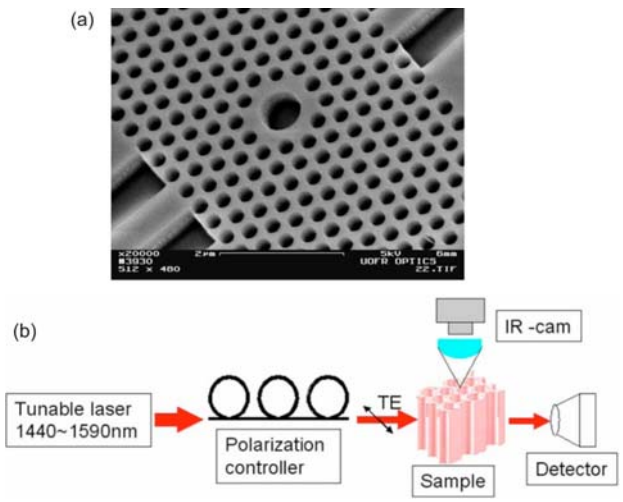

Figure 10 (online color at: www.biophotonics-journal.org) (**a**) SEM image of a photonic crystal microcavity device. The cavity is formed by increasing the center pore diameter. (**b**) Experimental set-up, composed of a light source, polarization control and detector, for resonance readout. Reprinted with permission from [46]. Copyright 2007, Optical Society of America.

To imitate an affinity-based biosensor, first bulk refractive index measurements with an ultracompact photonic crystal sensor are performed in [44], where the sensing area amounts to $\sim 10\,\mu m^2$. Here a resonance wavelength shift of ~ 0.4 nm for $\Delta n = 0.002$ is demonstrated corresponding to 200 nm/RIU. The authors also perform a time-resolved measurement and track the refractive index of a glycerol-water solution during the evaporation process. A further improvement in the bulk refractive index sensitivity was achieved in [45], where the authors use a microcavity sensor based on pillars. The pillar microcavity provides air-modes, whose electrical field distribution is more in the surrounding medium than in the pillar material. Hence, the mode has a higher overlap with the analyte and is more sensitive to refractive index changes. Moreover, the quality factor of the resonance was as high as 27,600, which allows resolving a refractive index difference of 3×10^{-4}.

Protein detection was first demonstrated in [46], where Lee et al. show the binding of glutaraldehyde and bovine serum albumin (BSA). To do so, they functionalize the internal surface of the photonic crystal holes for the specific binding with glutaraldehyde. With their setup they are able to detect a BSA monolayer with a total mass of 2.5 fg. Zlatanovic et al. [47] specify that they detect 4.5 fg of BSA. Furthermore, they demonstrate a molecular kinetics experiment with a photonic crystal microcavity biosensor. The sensor has a total area of 50 μm^2 with an effective detection area of less than 0.3 μm^2. Using the kinetic data they calculate the affinity constant of BSA to its counterpart.

Recently, new drop filter approaches were demonstrated. Here, a waveguide is positioned in the vicinity of photonic crystal cavities serving as the active sensing area of the device [48–50]. Light passing the waveguide couples evanescently to the cavity and a resonance is observed in the transmission or reflection spectrum through the waveguide. This allows a multiplex configuration, where multiple cavities can couple to one waveguide and detect more than one analyte with the appropriate surface functionalization. Dorfner et al. [51] show a protein drop filter sensor consisting of an L3 nanocavity coupled to a photonic crystal waveguide. The authors demonstrate a bulk refractive index sensitivity for the resonance wavelength of 103 nm/RIU and detect 4.0 ± 0.6 fg of BSA protein.

Kang et al. [52] use a similar cavity waveguide configuration, but enhance the sensitivity by introducing holes in the cavity. They increased the detection sensitivity up to 18% for bulk refractive index meas-

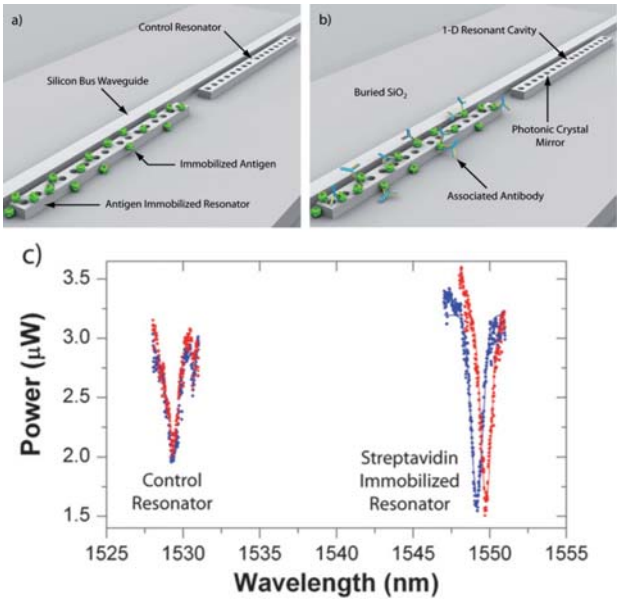

Figure 11 (online color at: www.biophotonics-journal.org) (**a**) 3D rendering of the device consisting of photonic crystal cavities and a silicon bus waveguide. One resonator is immobilized with streptavidin; a second resonator acts as a control. (**b**) Schematic with bound biotinylated antibody on the streptavidin surface. (**c**) The binding of the antibody leads to a redshift of the resonant wavelength without an influence on the control resonance. Reproduced from [53] with permission of The Royal Society of Chemistry.

urements, whereas for attachment of a small aminosilane molecule the detection sensitivity was increased by 44%.

In [53] the authors show a multiplex biosensor platform consisting of a one-dimensional photonic crystal microcavity array situated along a bus waveguide. Here, they use one resonator as the signal channel, which was immobilized with streptavidin, and another resonator as the control channel (Figure 11(a) and (b)). As each resonator is formed to possess a unique resonant wavelength, the signal and the control channel can be separated easily in the transmission channel. The bound biomolecule in the sensor channel results in a red shift of the resonant wavelength of the resonator, whereas no effect on the resonance of the control resonator is obtained (Figure 11(c)). The authors measure the binding of biotinylated antibody and estimate the device limit of detection to be 63 ag.

Theoretical investigations were carried out on how to enhance the sensitivity of these structures. In [54] finite-difference time-domain based simulations are used to optimize the overlap of the defect mode with the surrounding medium. Three arrangements are proposed for this purpose: reducing the slab thickness, introducing additional holes in the cavity or using a slot waveguide in the cavity. They show that all changes push the mode out of the slab material and enhance the interaction with the surrounding medium, which leads to a sensitivity increase of the sensor. The authors predict a sensitivity of up to 512 nm/RIU.

3. Pathogen Detection

Enzyme-linked immunosorbent assays (ELISA) are common for pathogen detection. Introduced more than 40 years ago [55], ELISA is still one of the most used antibody-based sensor methods. This method requires a high number of cells and requires at least several hours of incubation. Another widely used method for the detection of bacteria and viruses is the polymerase chain reaction (PCR), which requires complex sample preparation [56]. Therefore, there is a large potential for bacterial sensors that are rapid, compact and monitor the binding in real-time.

Photonic crystal biosensors were applied recently for whole cell sensing [57], for detection of human anti-dengue antibodies [58] and for living cell sensing [59]. This shows the general potential of photonic crystals in detection of unicellular organisms and viruses.

In [60] the authors use a microcavity approach with the defect created by increasing the central hole of the photonic crystal slab. They show the detection of a single latex particle with the size of a virus, which was in the cavity hole in Figure 10(a). They also theoretically show that a diameter variation of the particle results in a shift of the resonance. This can be used to distinguish between different pathogens.

The unspecific binding of bacteria to a grating-coupled planar optical waveguide is realized by Horvath et al. [61]. Their sensor is especially suitable for bacteria detection, as it has a nanoporous material as the substrate, which has a refractive index lower than water. This results in an increase in penetration depth of the evanescent wave. A protein layer (PLL, poly-L-lysine; 4 nm thickness) was coated on the surface to bind the E.coli bacteria on the grating. This protein layer provides a charge on the surface, which results in an electrostatic binding to bacterial cells [62]. The device setup is shown schematically in Figure 12. A laser beam is coupled to a polystyrene waveguide. A detector, which is attached to the edge of this waveguide, measures the amount of light coupling into the waveguide. Using a goniometer they scan the angle of incidence and find a resonance peak. The binding of E.coli to the surface results in a shift of the peak position. In their investigations they have an average density of bacteria attached to the surface of up to 12,400 cells/mm^2. The authors, however, estimate the detection limit of their sensor

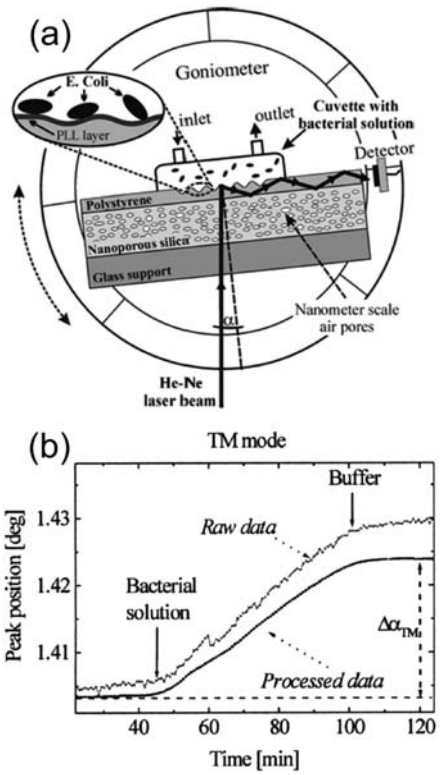

Figure 12 (**a**) Schematic of the device setup. (**b**) Peak position of the TM mode as a function of time. Reprinted with permission from [61]. Copyright 2003, Optical Society of America.

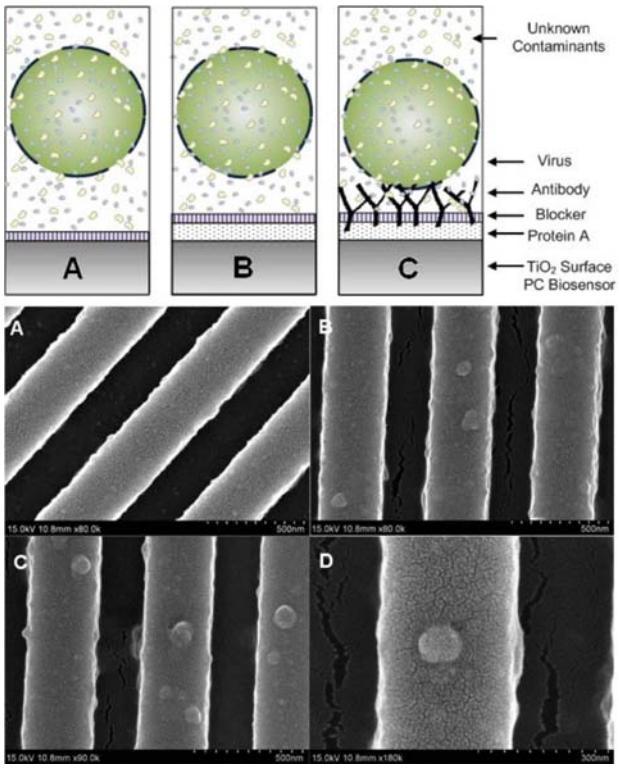

Figure 13 (online color at: www.biophotonics-journal.org) Top: Schematic of virus detection on the photonic crystal biosensor surface. (**a**) and (**b**) show different reference wells, and (**c**) depicts the active well with an anti-rotavirus-coated surface and bound rotavirus. Bottom: SEM images of the photonic crystal surface with bound rotavirus: (**a**) reference well without virus, (**b**) individual virus bound to the surface, (**c**) clusters of rotaviruses on the photonic crystal grating, and (**d**) zoomed image of a single rotavirus on the surface. © 2009 IEEE. Reprinted, with permission, from [63].

operated in the TM mode to be 60 cells/mm^2 based on the noise level of their system.

A disposable, rapid and label-free method to detect intact viable rotaviruses is demonstrated by Pineda et al. [63]. They use a photonic crystal slab sensor functionalized with anti-rotavirus antibodies. The detection limit of the system for viruses in partially purified solutions is lower than ~36 focus forming units (20 µl of 0.18×10^4 FFU/ml virus solution). This sensitivity limit is comparable to commercially available ELISA kits. The sensor system is incorporated into standard 96-, 384-, or 1536-well microplates [64]. Using an automated stage for parallel data collection from eight sensor wells at timed intervals, a 384-well microplate can be measured in less than 2 min. Figure 13 (top) shows the schematic picture of the specific binding of rotavirus to the antibody-coated surface. SEM images of the viruses bound to the photonic crystal slab are shown in Figure 13 (bottom).

4. On-Chip integration

In the last sections photonic crystal transducer concepts for biosensors were presented. Here, fabrication options are discussed that allow for future on-chip integration of the photonic crystal tranducers with microfluidics. Section 4.1 considers different fabrication methods for photonic crystals and Section 4.2 reviews on-chip integration demonstrators.

4.1 Fabrication methods

For the fabrication of 1D photonic crystals a range of well known thin-film stack fabrication methods is available: Thermal evaporation technique [65], electron beam evaporation [19, 66], sputtering [17, 67], low-pressure chemical vapor deposition [68], dip-coating [69], or spin-coating [70].

Common methods to fabricate 2D photonic crystal structures such as photonic crystal slabs, microcavities and waveguide structures are electron-beam lithography and reactive ion etching (RIE). The surface structures fabricated with this approach may be

replicated using nanoimprint lithography (NIL). The ability to use this low cost method for the fabrication of photonic crystal slabs for biosensor applications is shown in [71]. The grating structure is etched into the Si master by RIE. A PDMS cast mold is formed from the Si master stamp. This PDMS stamp is easy to release from the master and is used to pattern a low index layer on top of a glass substrate. The photonic crystal structure is completed by evaporation of a high-index layer consisting of TiO_2 (Figure 14). It is possible to pattern multiple grating regions at the same time. The authors show the patterning of 96 circular grating regions each with a 6 mm diameter corresponding to a standard 96-well microplate. The PDMS stamp can be used about ten times, before the pattern quality drops down [71]. It is therefore suitable for high-throughput fabrication. This method is also suitable for fabrication on flexible plastic substrates [72].

Gratings fabricated by injection molding were demonstrated by Cho et al. [73]. This method requires a durable metal stamp due to the high temperatures and pressure. A quartz master is used to fabricate a nickel stamp, which has the negative shape of the final grating. With this nickel stamp, the PMMA grating structures were fabricated by injection molding. A photograph and an SEM image of a PMMA grating fabricated by injection molding are shown in Figure 15.

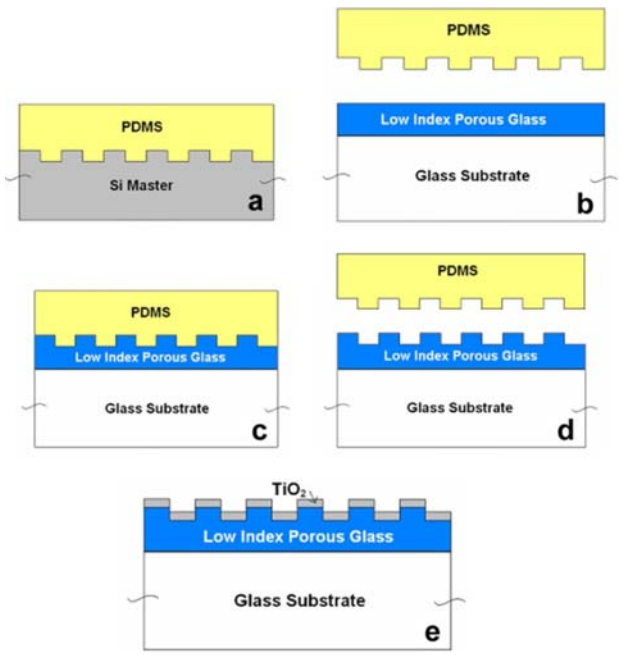

Figure 14 (online color at: www.biophotonics-journal.org) Fabrication Process: (**a**) PDMS cast mold formed with a Si master, (**b**) low-index sol-gel glass layer spin-coated on top of the glass substrate, (**c**) patterning of the low-index layer, (**d**) removal of the mold, and (**e**) complete device with evaporated high index layer of TiO_2. Reprinted from [71], Copyright 2007, with permission from Elsevier.

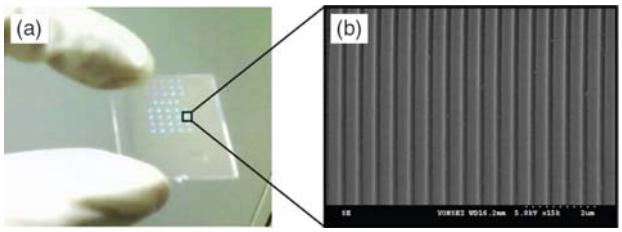

Figure 15 (online color at: www.biophotonics-journal.org) (**a**) Photograph and (**b**) SEM image of the grating fabricated by injection molding. Reprinted with permission from [73]. Copyright © American Scientific Publishers.

Injection molding is the most suitable process for mass production of polymer nanostructures.

4.2 System demonstrations

The novel fabrication processes including nanoimprint lithography and injection molding open the door for biosensors on-chip. Using microfluidic channels small volumes of analyte can be transported to the sensing region.

The possibility to integrate a microfluidic network and photonic crystal biosensors into a 96-well microplate is shown by Choi et al. [74]. To fabricate photonic crystal structures in the nanometer range and microfluidic channels with a minimum channel width of 150 μm, a replica molding method is used [75]. To obtain a negative pattern in a silicon wafer, lithography methods and reactive ion etching are used. With this master a 250 μm thick flexible polyethylene terephthalate (PET) substrate is patterned. By evaporating a TiO_2 layer on the surface of the polymer replica, the sensor structure is completed. The open microfluidic channels are sealed with a separate PET sheet. 88 parallel flow channels with photonic crystal structure and 8 common inlets/outlets are integrated on the bottom of a 96-well microplate as shown in Figure 16. Only 220 nL are necessary to fill 11 flow channels. The ability to detect protein-protein interactions is demonstrated. The authors suggest that this system can be used with 11 different ligands, which are subsequently exposed to a single analyte.

A single chip fabrication method is shown by Jugessur et al. [76]. Here, a silicon-on-insulator chip is fabricated including a grating structure as well as a fluidic network with reservoirs. This chip is integrated with a PDMS chip, which can be replaced after a single use. A schematic of the chip design is shown in Figure 17. The computed sensitivity of the device is 5.5×10^{-3} nm^{-1} for refractive index meas-

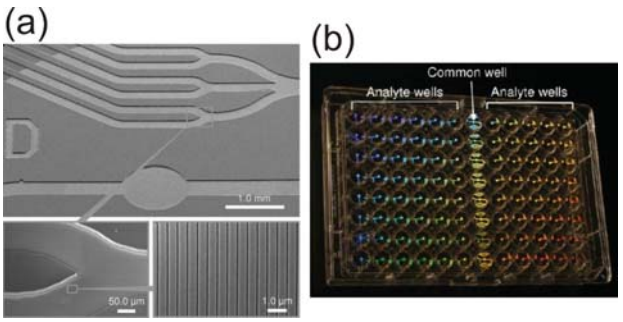

Figure 16 (online color at: www.biophotonics-journal.org) (**a**) SEM image of the microfluidic channels and photonic crystal structures molded in the polymer replica. (**b**) Photograph of the fabricated polymer microfluidic network with integrated photonic crystal structures attached on the bottom of a 96-well microplate. Reproduced from [74] with permission of The Royal Society of Chemistry.

urements. This sensitivity is not confirmed experimentally.

An optofluidic integration architecture is shown for instance by Erickson et al. [77]. They demonstrate the nanofluidic addressing of a single row of holes within the photonic crystal lattice.

The detection of dissolved avidin using functionalized slotted photonic crystal cavities with integrated microfluidics is shown by Scullion et al. [78]. They are able to detect a surface mass coverage of 60 pg/mm^2 with a cavity sensing area of 2.2 μm^2.

Another method to integrate nanofluidics in a photonic crystal sensor is shown by Huang et al. [35]. A free-standing photonic crystal slab is sealed into a chamber as shown in Figure 18. The nano-scale hole

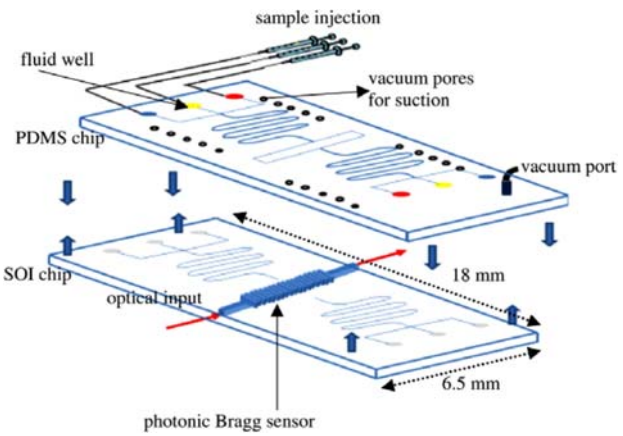

Figure 17 (online color at: www.biophotonics-journal.org) Schematic diagram of the device consisting of a silicon-on-insulator (SOI) chip and a PDMS chip. The grating structure is integrated with fluidic channels and reservoirs for fluidic sensing. Reprinted from [76], Copyright 2009, with permission from Elsevier.

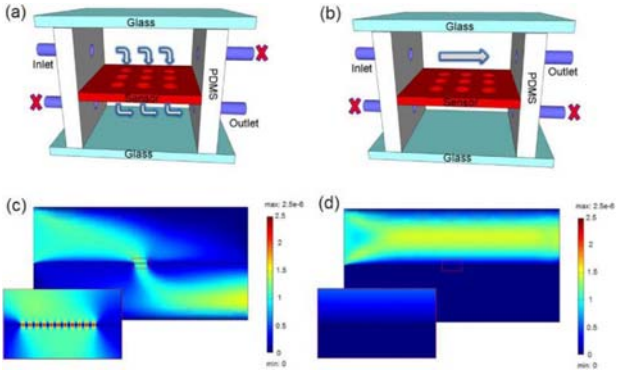

Figure 18 (online color at: www.biophotonics-journal.org) (**a**) and (**b**): Schematic diagram of the device. (**a**) Solution directed to the structure surface is guided through the nano-scale hole array and flows to the bottom channel and (**b**) conventional flow scheme, where the flow stream passes over the sensor surface. (**c**) and (**d**): Velocity distributions of solution for the proposed and the conventional flow scheme, respectively. Insets show the flow profiles around the photonic crystal structure in detail. Reprinted with permission from [35]. Copyright 2009, Optical Society of America.

array offers the possibility to control the flow between the top and the bottom of the chamber. With bulk measurements a sensitivity of 510 nm/RIU is demonstrated. The authors state that this device is able to detect minute amounts of analyte from small quantities of biological samples.

Apart from the integration of microfluidic channels and transducers another challenge for successful on-chip biosensing is the need for multiplexing several analytes. As discussed in chapter 2.4 Mandal et al. [53] showed a multiplex biosensor platform for detection of three different cytokines. Lai et al. [79] demonstrated the possibility to integrate microcavities of different sizes for biosensing applications. The different cavity lengths allows for multiplexed detection of antibodies. Multiplexing can also be used for error correction and therefore improve the measurement accuracy [80].

The demonstrated systems may be differentiated by the way the analytes are evaluated in the measurement volume. In case of a well plate multiple photonic crystal structures and multiple measurements in space are necessary. With an imaging readout system, all spatial positions may be evaluated simultaneously. Multiple measurements in time are needed in case of multiple microfluidic channels or different biosensors along the same channel. This also requires the movement of the sample liquid across the chip. On the other hand, in a microfluidic system the sample is protected from air exposure and filtering capability can be added. This is of particular importance for the evaluation of whole-blood samples on-chip.

These first systems demonstrate the potential of on-chip system integration for photonic crystal biosensors. This research area is still at the beginning and large progress is expected over the next years.

5. Conclusion

The property of photonic crystals to confine light enhances the light-matter interaction and offers a high potential for on-chip biosensing applications. In Table 1 we summarize the highest sensitivities and the lowest detection limits denoted as refractive index change, analyte concentration and surface mass coverage for the photonic crystal biosensors reviewed here. In this table only experimental results are considered and not all references gave values for all quantities such that we could only compare the stated values.

The resonance sensitivities (except for the 1D photonic crystal sensors) are rather low in comparison to surface plasmon resonance (SPR) sensors [81]. However, the sensor's performance is also a function of the quality factor. Photonic crystal sensors with their relatively high quality factor deliver comparable results to SPR sensors regarding the detectable analyte concentration [81, 82]. With commercially available SPR sensors a surface mass coverage of 0.5 pg/mm^2 is detectable [83].

One advantage of photonic crystal biosensors is their small sensing region such that small sample volumes containing low concentrations of biomolecules are sufficient.

1D photonic crystal biosensors are able to perform highly sensitive measurements of biomolecular interactions. This sensing method can resolve small molecule binding with high signal-to-noise ratio and was able to detect low mass adsorption on the surface with a high sensitivity [19].

For biosensors with photonic crystal slabs, the sensitivity can be greatly enhanced through the incorporation of nanorod structures on the surface [30] or through roughening of the surface [31]. Both methods result in an increased effective surface area and therefore lead to a higher sensitivity. Also the operation at near-ultraviolet wavelengths leads to an improvement of the sensitivity [36]. As the TM and TE polarization states provide different resonance peaks, a separate reference channel is not necessary [28]. This allows for a smaller sensing region.

Ultracompact monitoring of biomolecular interactions was shown for photonic crystal microcavity biosensors. A sensing area of 1.7 μm^2 was demonstrated by Dorfner et al. [51].

Another challenge is the multiplex detection. Most of the systems highlighted here are not able to detect more than one analyte. A solution is demonstrated for instance by Mandal et al. [53]: The system consisting of a bus waveguide next to an array of different 1D cavity resonators is utilized for the multiplex detection of three different cytokines. Cunningham et al. [64] showed the integration of photonic crystal structures into a regular 1536-well microplate.

Nevertheless, there is a limit to improving the sensitivity and detection limit due to ambient temperature fluctuations. Measuring refractive index changes below 10^{-6} RIU requires thermal stabilization of the system. Changing the temperature will cause a change in the index of the measured water-based analyte solution. Incorporating reference channels [19] or temperature-stable cavities [84] are examples for overcoming these limits.

Most of the photonic crystal sensors reported to date focused on proof-of-principle demonstration. While the system from Cunningham et al. is commercially available [64], other systems have yet to demonstrate their applicability in real-world analysis. This also explains the differences in the values given in Table 1. The photonic crystal waveguide sensor systems and the photonic crystal cavity sensor systems are not yet optimized to their full potential.

In order to achieve a photonic crystal biosensor with a low detection limit the following rules should be regarded:

Table 1 Sensitivities and detection limits of the four different types of photonic crystal biosensors. Please note that the best values for the experimental sensors reviewed in this article are given and that these values were obtained in different types of experiments (different analytes, different wavelengths, different electronics, etc.). Furthermore, not all reviewed papers presented all values such that we could only consider the mentioned values.

Biosensing system	Sensitivity $\Delta\lambda/\Delta n$ (nm/RIU)	Refractive index Δn (RI)	Analyte concentration (g/mL)	Surface mass coverage (g/mm^2)
1D photonic crystals	1840 [19]	1×10^{-8} [19]		60×10^{-15} [18]
Photonic crystal slabs	510 [35]	3.4×10^{-5} [23]	1×10^{-9} [23]	1×10^{-12} [26]
Photonic crystal waveguides	120 [43]	3×10^{-3} [42]	10×10^{-9} [42]	6×10^{-9} [42]
Photonic crystal cavities	350 [45]	3×10^{-4} [45]		50×10^{-12} [60]

- The present biomolecules should be concentrated to a small functionalized detection volume in order to achieve the largest possible absolute refractive index change.
- To obtain a high sensitivity the optical read-out mode should match the detection volume in height and lateral extension. This may be achieved by choice of the mode (wavelength, polarization), design of the photonic crystal structure and design of the optical read-out.
- The system should be low noise.

All four types of photonic crystal biosensors reviewed here have the potential for on-chip integration. With new fabrication processes such as nanoimprint lithography and injection molding on-chip integration is within reach. The assembly of microfluidic channels in the micrometer range and photonic crystal structure in the nanometer range on a single chip in a low-cost fabrication process were already demonstrated [74, 75]. On-chip photonic crystal biosensors are suitable for rapid and accurate medical diagnoses or for pathogen detection. This opens up new possibilities in point-of-care diagnoses with rapid progress expected in the next years.

Daniela Threm received the diploma degree in electrical and information engineering and business management from the Christian-Albrechts-Universität zu Kiel, Germany, in 2009, where she is now pursuing her Ph.D. in the department of electrical and information engineering. Her research interests include organic optoelectronic devices and integrated systems as well as biophotonics.

Yousef Nazirizadeh received the master's degree in electrical engineering with the major of photonics from the Royal Institute of Technology (KTH) in Stockholm, Sweden in 2005, and the Ph.D. degree in electrical engineering from Karlsruher Institute of Technology (KIT), Germany in 2010. Now he has a post-doctoral position in the Integrated Systems and Photonics Group at the Christian-Albrechts-Universität zu Kiel, Germany, with research interests including bio- and nanophotonics.

Martina Gerken received the Dipl.-Ing. degree in electrical engineering from the University of Karlsruhe, Germany, in 1998, and the Ph.D. degree in electrical engineering from Stanford University, Stanford, CA, USA in 2003. From 2003 to 2008 she was an Assistant Professor at the University of Karlsruhe, Germany. In 2008 she was appointed as a full Professor of electrical engineering and head of the Integrated Systems and Photonics Group at the Christian-Albrechts-Universität zu Kiel, Germany.

References

[1] D. Fraser, Medical Device Technology **5**, 38–41 (1994).
[2] H. M. Haake, A. Schütz, and G. Gauglitz, Fresenius Journal of Analytical Chemistry **366**, 576–585 (2000).
[3] J. M. Perkel, Science **325**, 1561–1563 (2009).
[4] S. P. Mohanty and E. Kougianos, IEEE Potentials **25**, 35–40 (2006).
[5] E. Yablonovitch, Physical Review Letters **58**, 2059–2062 (1987).
[6] S. John, Physical Review Letters **58**, 2486–2489 (1987).
[7] J. D. Joannopoulos, P. R. Villeneuve, and S. Fan, Nature **386**, 143–149 (1997).
[8] J. D. Jannopoulos, S. G. Johnson, J. N. Winn, R. D. Meade, Photonic Crystals – Molding the Flow of Light, second Edition (Princeton University Press, New Jersey, 2008).
[9] S. Fan, P. Villeneuve, J. Joannopoulos, and E. Schubert, Physical Review Letters **78**, 3294–3297 (1997).
[10] J. Piehler, A. Brecht, and G. Gauglitz, Analytical Chemistry **68**, 139–143 (1996).
[11] G. Gauglitz, Analytical and Bioanalytical Chemistry **381**, 141–155 (2005).
[12] G. M. Whitesides, Nature **442**, 368–373 (2006).
[13] N. A. Mortensen, S. Xiao, and J. Pedersen, Microfluidics and Nanofluidics **4**, 117–127 (2007).
[14] H. Inouye, M. Arakawa, J. Y. Ye, T. Hattori, H. Nakatsuka, and K. Hirao, IEEE Journal of Quantum Electronics **38**, 867–871 (2002).
[15] W. M. Robertson, Journal of Lightwave Technology **17**, 2013–2017 (1999).
[16] F. Villa, L. E. Regalado, F. Ramos-Mendieta, J. Gaspar-Armenta, and T. Lopez-Ríos, Optics Letters **27**, 646–648 (2002).
[17] V. N. Konopsky and E. V. Alieva, Analytical Chemistry **79**, 4729–4735 (2007).
[18] Y. Guo, C. Divin, A. Myc, F. L. Terry, Jr., J. R. Baker, Jr., T. B. Norris, and J. Y. Ye, Optics Express **16**, 11741–11749 (2008).

[19] Y. Guo, J. Y. Ye, C. Divin, B. Huang, T. P. Thomas, J. R. Baker, Jr., and T. B. Norris, Analytical Chemistry **82**, 5211–5218 (2010).
[20] S. Fan and J. Joannopoulos, Physical Review B **65**, 1–8 (2002).
[21] S. G. Johnson, S. Fan, P. R. Villeneuve, J. D. Joannopoulos, and L. A. Kolodziejski, Physical Review B **60**, 5751–5758 (1999).
[22] K. Vahala (ed.), Optical Microcavities – Advanced Series in Applied Physics (World Scientific Publishing, Singapore, 2004).
[23] B. Cunningham, P. Li, B. Lin, and J. Pepper, Sensors and Actuators **81**, 316–328 (2002).
[24] L. L. Chan, S. L. Gosangari, K. L. Watkin, and B. T. Cunningham, Apoptosis **12**, 1061–1068 (2007).
[25] L. Chan, S. Gosangari, K. Watkin, and B. Cunningham, Sensors and Actuators B: Chemical **132**, 418–425 (2008).
[26] B. T. Cunningham and L. Laing, Expert Review of Proteomics **3**, 271–281 (2006).
[27] L. L. Chan, M. Pineda, J. T. Heeres, P. J. Hergenrother, and B. T. Cunningham, ACS Chemical Biology **3**, 437–348 (2008).
[28] R. Magnusson, D. Wawro, S. Zimmerman, and Y. Ding, Sensors **11**, 1476–1488 (2011).
[29] M. El Beheiry, V. Liu, S. Fan, and O. Levi, Optics Express **18**, 22702–22714 (2010).
[30] W. Zhang, N. Ganesh, I. D. Block, and B. T. Cunningham, Sensors and Actuators B: Chemical **131**, 279–284 (2008).
[31] C.-S. Jao and H. Y. Lin, Applied Optics **50**, 5139 (2011).
[32] I. D. Block, L. L. Chan, and B. T. Cunningham, Sensors and Actuators B: Chemical **120**, 187–193 (2006).
[33] L. Shi, P. Pottier, Y.-A. Peter, and M. Skorobogatiy, Optics Express **16**, 17962–17971 (2008).
[34] L. Shi, P. Pottier, M. Skorobogatiy, and Y.-A. Peter, Optics Express **17**, 10623–10632 (2009).
[35] M. Huang, A. A. Yanik, T.-Y. Chang, and H. Altug, Optics Express **17**, 24224–24233 (2009).
[36] N. Ganesh, I. D. Block, and B. T. Cunningham, Applied Physics Letters **89**, 023901 (2006).
[37] Y. Nazirizadeh, U. Bog, S. Sekula, T. Mappes, U. Lemmer, and M. Gerken., Optics Express **18**, 19120–19128 (2010).
[38] Y. Nazirizadeh, J. G. Müller, U. Geyer, D. Schell, E.-B. Kley, A. Tünnermann, U. Lemmer, and M. Gerken, Optics Express **16**, 7153–7160 (2008).
[39] S. G. Johnson, P. R. Villeneuve, S. Fan, and J. Joannopoulos, Physical Review B **62**, 8212 (2000).
[40] M. Lončar, D. Nedeljkovic, T. Doll, J. Vuckovic, A. Scherer, and T. P. Pearsall, Applied Physics Letters **77**, 1937 (2000).
[41] J. Topol'ančik, P. Bhattacharya, J. Sabarinathan, and P.-C. Yu, Applied Physics Letters **82**, 1143 (2003).
[42] N. Skivesen, A. Têtu, M. Kristensen, J. Kjems, L. H. Frandsen, and P. I. Borel, Optics Express **15**, 3169–3176 (2007).
[43] S. C. Buswell, V. A. Wright, J. M. Buriak, V. Van, and S. Evoy, Optics Express **16**, 15949–15957 (2008).
[44] E. Chow, A. Grot, L. W. Mirkarimi, M. Sigalas, and G. Girolami, Optics Letters **29**, 1093–1095 (2004).
[45] T. Xu, N. Zhu, M. Y.-C. Xu, L. Wosinski, J. S. Aitchison, and H. E. Ruda, Optics Express **18**, 5420–5425 (2010).
[46] M. R. Lee and P. M. Fauchet, Optics Letters **32**, 3284–3286 (2007).
[47] S. Zlatanovic, L. W. Mirkarimi, M. M. Sigalas, M. A. Bynum, E. Chow, K. M. Robotti, G. W. Burr, S. Esener, and A. Grot, Sensors and Actuators B: Chemical **141**, 13–19 (2009).
[48] D. F. Dorfner, T. Hürlimann, T. Zabel, L. H. Frandsen, G. Abstreiter, and J. J. Finley, Applied Physics Letters **93**, 181103 (2008).
[49] S. Pal, E. Guillermain, R. Sriram, B. Miller, and P. M. Fauchet, Proc. SPIE **7553**, 755304 (2010).
[50] S. Mandal and D. Erickson, Optics Express **16**, 1623–1631 (2008).
[51] D. Dorfner, T. Zabel, T. Hürlimann, N. Hauke, L. Frandsen, U. Rant, G. Abstreiter, and J. Finley, Biosensors & Bioelectronics **24**, 3688–3692 (2009).
[52] C. Kang, C. T. Phare, Y. A. Vlasov, S. Assefa, and S. M. Weiss, Optics Express **18**, 27930–27937 (2010).
[53] S. Mandal, J. M. Goddard, and D. Erickson, Lab on a Chip **9**, 2924–2932 (2009).
[54] S.-H. Kwon, T. Sünner, M. Kamp, and A. Forchel, Optics Express **16**, 11709–11717 (2008).
[55] E. Engvall and P. Perlmann, Immunochemistry **8**, 871–874 (1971).
[56] C. Drosten, S. Göttig, S. Schilling, M. Asper, M. Panning, H. Schmitz, and S. Günther, Journal of Clinical Microbiology **40**, 2323–2330 (2002).
[57] N. Zaytseva, W. Miller, V. Goral, J. Hepburn, Y. Fang, Applied Physics Letters **98**, 163703 (2011).
[58] M. C. Y. Huang, C. F. R. Mateus, J. E. Foley, R. Beatty, B. T. Cunningham, and C. J. Chang-Hasnain, Photonic Technology Letters **20**, 443–445 (2008).
[59] Y. Fang, A. M. Ferrie, N. H. Fontaine, J. Mauro, and J. Balakrishnan, Biophysical Journal **91**, 1925–1940 (2006).
[60] M. R. Lee and P. M. Fauchet, Optics Express **15**, 4530–4535 (2007).
[61] R. Horváth, H. C. Pedersen, N. Skivesen, D. Selmeczi, and N. B. Larsen, Optics Letters **28**, 1233–1235 (2003).
[62] Y. H. An and R. J. Friedman, Journal of Biomedical Materials Research **43**, 338–348 (1998).
[63] M. F. Pineda, L. L.-Y. Chan, T. Kuhlenschmidt, C. J. Choi, M. Kuhlenschmidt, and B. T. Cunningham, IEEE Sensors **9**, 470–477 (2009).
[64] B. T. Cunningham, P. Li, S. Schulz, B. Lin, C. Baird, J. Gerstenmaier, C. Genick, F. Wang, E. Fine, and L. Laing., Journal of Biomolecular Screening **9**, 481–490 (2004).
[65] M. J. Bloemer and M. Scalora, Applied Physics Letters **72**, 1676 (1998).
[66] G. Ma, J. Shen, Z. Zhang, Z. Hua, and S. H. Tang, Optics Express **14**, 858–865 (2006).
[67] H.-Y. Lee, H. Makino, T. Yao, and A. Tanaka, Applied Physics Letters **81**, 4502 (2002).

[68] M. Patrini, M. Galli, M. Belotti, L. C. Andreani, G. Guizetti, G. Pucker, A. Lui, P. Bellutti, and L. Pavesi, Journal of Applied Physics **92**, 1816 (2002).
[69] J. Bellessa, S. Rabaste, J. C. Plenet, J. Dumas, J. Mugnier, and O. Marty, Applied Physics Letters **79**, 2142 (2001).
[70] K. M. Chen, A. W. Sparks, H.-C. Luan, D. R. Lim, K. Wada, and L. C. Kimerling, Applied Physics Letters **75**, 3805 (1999).
[71] I. Block, L. Chan, and B. Cunningham, Microelectronic Engineering **84**, 603–608 (2007).
[72] I. D. Block, M. Pineda, C. J. Choi, and B. T. Cunningham, Sensors Journal, IEEE **8**, 1546–1547 (2008).
[73] E. Cho, B. Kim, S. Choi, J. Han, J. Jin, J. Han, J. Lim, Y. Heo, S. Kim, G. Y. Sung, and S. Kang, Journal of Nanoscience and Nanotechnology **11**, 417–421 (2011).
[74] C. J. Choi and B. T. Cunningham, Lab on a Chip **7**, 550–556 (2007).
[75] C. J. Choi, and B. T. Cunningham, Lab on a Chip **6**, 1373–1380 (2006).
[76] A. S. Jugessur, J. Dou, J. S. Aitchison, R. M. De La Rue, and M. Gnan, Microelectronic Engineering **86**, 1488–1490 (2009).
[77] D. Erickson, T. Rockwood, T. Emery, A. Scherer, and D. Psaltis, Optics Letters **31**, 59–61 (2006).
[78] M. G. Scullion, A. Di Falco, and T. F. Krauss, Biosensors & Bioelectronics **27**, 101–105 (2011).
[79] W.-C. Lai, S. Chakravarty, Y. Zou, and R. T. Chen, Optics Letters **37**, 1208–1210 (2012).
[80] S. Pal, E. Guillermain, R. Sriram, B. L. Miller, and P. M. Fauchet, Biosensors & Bioelectronics **26**, 4024–4031 (2011).
[81] J. Homola, S. S. Yee and G. Gauglitz, Sensors and Actuators B: Chemical **54**, 3–15 (1999).
[82] J. Homola, Analytical and Bioanalytical Chemistry **377**, 528–539 (2003).
[83] D. G. Myszka, Analytical Biochemistry **329**, 316–323 (2004).
[84] C. Karnutsch, C. L. C. Smith, A. Graham, S. Tomljenovic-Hanic, R. McPhedran, B. J. Eggleton, L. O'Faolain, T. F. Krauss, S. Xiao, and N. A. Mortensen, Applied Physics Letters **94**, 231114 (2009).

